

Transmembrane Fragment Structures of Amyloid Precursor Protein Depend on Membrane Surface Curvature

Laura Dominguez,[†] Stephen C. Meredith,[‡] John E. Straub,^{*,†} and David Thirumalai[§]

[†]Department of Chemistry, Boston University, Boston, Massachusetts 02215, United States

[‡]Department of Biochemistry and Molecular Biology and Department of Pathology, The University of Chicago, Chicago, Illinois 60637, United States

[§]Department of Chemistry and Biochemistry and Biophysics Program, University of Maryland, College Park, Maryland 20742, United States

S Supporting Information

ABSTRACT: The amyloid β ($A\beta$) peptide associated with Alzheimer's disease results from processing of the amyloid precursor protein (APP) by secretases. Cleavage of APP by β -secretase produces a 99 amino acid C-terminal fragment of APP (C99) consisting of a single transmembrane (TM) helix. Simulations of C99 congeners and structural studies of C99 in surfactant micelles and lipid vesicles have shown that a key peptide structural motif is a prominent "GG kink," centered at two glycines dividing the TM helix. The flexibility of the GG kink is important in the processing of C99 by γ -secretase. We performed multiscale simulations of C99_{15–55} in a DPC surfactant micelle and POPC lipid bilayer in order to elucidate the role of membrane surface curvature in modulating the peptide structure. C99_{15–55} in a DPC surfactant micelle possesses a "GG kink," in the TM domain near the dynamic hinge located at G37/G38. Such a kink is not observed in C99_{15–55} in a POPC lipid bilayer. Intramolecular interaction between the extracellular and TM domains of C99_{15–55} is enhanced in the micelle environment, influencing helical stability, TM helix extension, exposure to water, and depth of insertion in the lipophilic region. Our results show that the fluctuations of the structural ensemble of APP are strongly influenced by membrane surface curvature.

There has been a great deal of interest in understanding the structure and kinetics of aggregation of amyloid β ($A\beta$) peptides associated with Alzheimer's disease (AD).^{1,2} In contrast, much less attention has been paid to the production of $A\beta$ peptide, which occurs by proteolytic cleavage of the membrane associated APP-C99 (C99), a 99 amino acid C-terminal fragment of the amyloid precursor protein (APP) by γ -secretase.^{3–5}

C99 consists (Figure 1) of a central TM helical domain (K28–K53/K699–K724 for C99/APP) flanked by an extracellular N-terminal region, including asparagine glycosylation sites and a juxtamembrane (JM) helix (Q15–V24/Q686–V695), and an intracellular domain, including a C-terminal helix (T90–N99/T761–N770).^{3–6} Cleavage by γ -secretase is initiated at the ϵ -site (T49/L49) and precedes processively until termination. The point of termination varies leading to $A\beta$ lengths of 38 to 43 amino acids.⁷ $A\beta$ 40, the dominant isoform,^{8,9} and $A\beta$ 42,

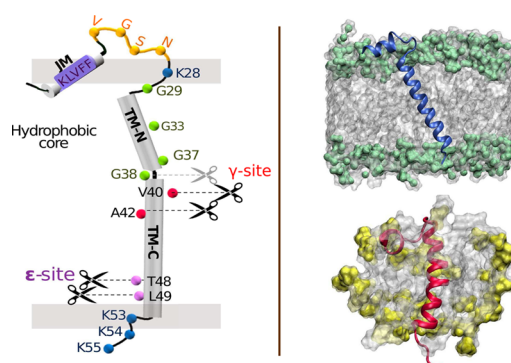


Figure 1. (Left) Schematic of C99 showing key sequence information, likely secondary structure regions, ϵ - and γ -cleavage sites, and approximate insertion within the membrane bilayer. The break in the TM helix at the "GG kink" between G37/G38 is indicated. (Right) Depiction of C99_{15–55} monomer in a POPC lipid bilayer (above) showing an average tilt angle of 22.5° with respect to the bilayer normal and (below) C99_{15–55} in a DPC micelle. The phosphocholine group is shaded green (POPC) or yellow (DPC).

considered the most amyloidogenic isoform, normally occur in a 10:1 ratio.^{10,11} How changes in C99 sequence and variations in membrane environment impact the distribution of $A\beta$ isoforms is critical to our understanding of the etiology of AD.^{12,13}

We had previously predicted¹⁴ that the TM helix was rendered flexible through the presence of a dynamic "GG hinge" at G37/G38 using simulations of monomeric C99_{1–55} in a model bilayer. The helix preceding G37 (referred to as Domain B) was found to be less helical than the helix following G38 (referred to as Domain C). We also proposed that the reduced helicity in Domain B facilitated close interpeptide backbone association and C_{α} hydrogen bonding stabilizing the homodimer. Subsequent experiments quantitatively confirmed these two key predictions.⁶

Based on structural studies of C99 in micelles,^{6,15} it has been conjectured that the TM helix flexibility, due to the presence of a dynamic GG hinge (see Figure 1), may facilitate interaction of C99 with the active site of γ -secretase.¹⁶

Although a structural kink, i.e., a nondynamic bend in the structure, might be considered a constraint on the passage of C99

Received: October 31, 2013

Published: December 23, 2013

toward the active site, possibly signaling termination of cleavage, the presence of a dynamic hinge is expected to facilitate passage of the peptide during processive cleavage. This finding is in accord with our predictions.¹⁴

Recent H/D exchange experiments on the C99 peptide, complemented by molecular dynamics simulations of C99_{28–55} in a POPC bilayer, showed enhanced H/D exchange in the N-terminal region of the TM domain (TM-N helix, domain B) relative to the C-terminal portion (TM-C helix, domain C).¹⁷ The finding is in agreement with experimental studies of C99 monomer in LMPG micelles.⁶

It should be noted that our simulations¹⁴ and those of Pester et al.¹⁷ were performed in bilayer environments, whereas the insightful NMR experiments used C99 in spatially constrained micelles.⁶ The difference raises a crucial question, namely, how does the membrane, especially the surface curvature, effect the conformational fluctuations of C99?

To answer this open question quantitatively, we performed simulations of the structure and stability of monomeric C99_{15–55} in POPC lipid bilayer and DPC surfactant micelle environments. We show that although micelles are an important model system for probing the structure of C99, the extent of fluctuations in C99, proposed to be crucial in the A β product distribution upon cleavage by secretases, depends strongly on membrane surface curvature. Our results provide a detailed picture of the C99_{15–55} structural ensemble and the potential role for changes in structure to influence the function and processing of this critical APP.

The structural ensemble of C99_{15–55} was characterized in 1-palmitoyl-2-oleoyl-*sn*-glycero-3-phosphocholine (POPC) lipid bilayer and dodecylphosphocholine (DPC) surfactant micelle environments. To ensure that our conclusions are robust, a multiscale computational approach was employed combining μ s time scale coarse-grained (CG) models of the protein, lipids, and solvent using the MARTINI force field^{18,19} and 100 ns time scale all-atom CHARMM36 force field models for the protein, membrane, and solvent (see Supporting Information for details).^{20,21} The CG simulations were used to assess the long-time dynamics and the role of fluctuations in the protein and lipid conformational ensemble.^{22–25} All-atom simulations provided an atomically detailed picture of the protein structure, protein–membrane interactions, the lipid/water interface, and water dynamics allowing for comparison with experimental data for C99 in lysomyristoylphosphatidylglycerol (LMPG) micelles at pH 6.5 and 45C (see Figure 1).

Comparison of the depth of insertion in our simulations (see Figure 2 and Supporting Information for details) with experiments of Sanders et al., derived from NMR experiments with water-soluble and lipophilic paramagnetic probes,¹⁵ shows good agreement.

Our study was designed to compare the impact of geometry and membrane surface curvature on peptide structure, using a POPC lipid and DPC surfactant that share similar zwitterionic head groups and alkyl chain lengths. Because the experimental results were obtained for C99 in LMPG micelles,⁶ which have an anionic (rather than zwitterionic) headgroup and longer (by 2 carbons) alkyl chain length, a direct comparison with our predictions cannot be made.

The simulation results for C99_{15–55} in a DPC micelle capture the essential features of the experimental measurements for full length C99 in an LMPG micelle (see Figure 2). Differences primarily occur near the N- and C-terminal regions of C99_{15–55} (midsequence in full-length C99) and for residues localized near

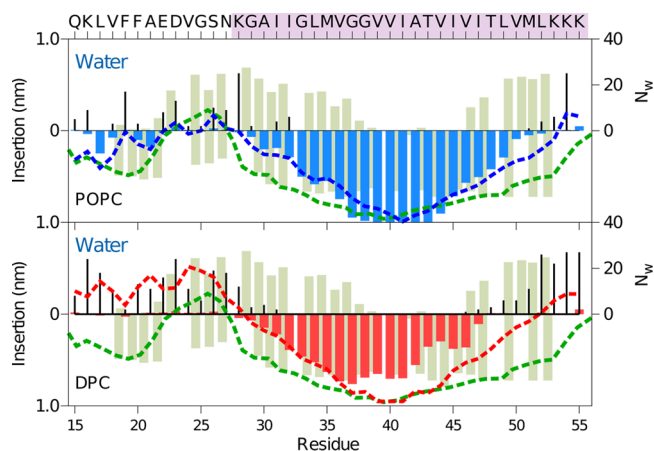


Figure 2. Water and lipid accessibility of each residue of C99_{15–55} in POPC bilayer (top) and a DPC micelle (bottom) derived from all-atom simulations. The green bars depict the degree of contact with the water-soluble paramagnetic probe (Gd-DTPA, positive values) and the lipophilic probe (16-DSA, negative values) for C99 in LMPG micelles.¹⁵ The EPR power saturation data from experiments are in green dashed lines. Shown for comparison are simulation results for the depth of insertion in the lipid phase (colored bar), number of water molecules, N_w (black lines) within 4 Å of each amino acid, and the insertion depth calculated by taking the location of the membrane width or the micelle size for POPC (blue dashed line) and DPC (red dashed line). The TM sequence is marked with orchid shading.

the headgroup region (chemically distinct in neural DPC and anionic LMPG). Comparison of the results between the bilayer and micelle (Figure 2, top and bottom) shows the quantitative difference, which is the first indication that the surface curvature of the membrane affects the conformational ensemble of C99_{15–55}. We observe remarkable agreement in JM helix insertion and peptide solvation between the all-atom and CG simulations in POPC bilayer (Figure 2 and S2). Having established that our simulations represent the water and lipid accessibility in a micellar environment, we further examined the role of membrane surface curvature on other structural features. In simulations, residues at the interface in the DPC micelle present higher accessibility to water than the same residues in the POPC bilayer. Our simulations in a POPC bilayer show that the JM domain of C99_{15–55} (residues Q15–N27) is localized at the membrane interface, which allows the central hydrophobic residues V¹⁷FFA²⁰ to insert into the headgroup region. In contrast, in the DPC micelle the residues of the JM domain are significantly more accessible to water. In both the bilayer and micelle environments, K28 is localized near the interface. However, in the DPC micelle the C-terminal amino acids L⁴⁹VMLKKK⁵⁵ are significantly more exposed to water than in the POPC bilayer.

Figure 3 relates fluctuations in the TM and JM helical regions for C99_{15–55} in the POPC bilayer (upper) and DPC micelle (lower) derived from simulation and compared with measures of helicity from experimental studies of C99 in an LMPG micelle at pH 6.5 and 45C.¹⁵ In both environments, two helical regions are observed with the interhelical region located at V²³GSN²⁷, which often forms bends in A β fibrils and monomers.²⁶ However, there are also significant differences. In the POPC bilayer the integrity of the JM helix is somewhat greater than in the DPC micelle. Moreover, there is a critical break in the TM helix observed in both simulation and experiment in the micelle environment near G37/G38 that is largely absent for the peptide in the POPC

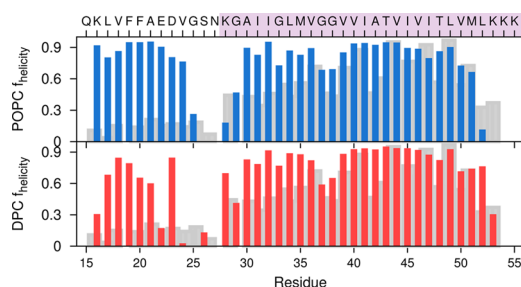


Figure 3. The α -helicity of each residue in the C99₁₅₋₅₅ monomer simulation in DPC micelle (red) and POPC bilayer (blue) derived from all-atom simulations. The α -helical residues were assigned with DSSP. Shown in gray is the degree of helicity determined experimentally from C α chemical shifts for the C99 peptide in LMPG micelles.¹⁵

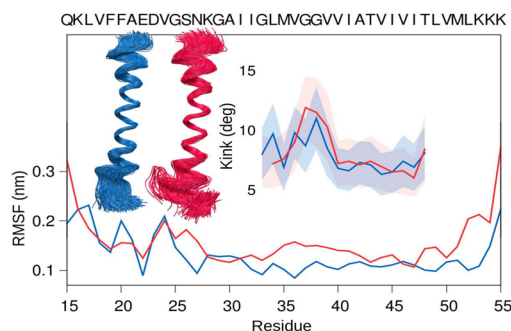


Figure 4. Measurement of the (inset) structural kink derived from all-atom simulations in the peptide and (lower) root-mean-square fluctuations in C α atoms as a function of residue for the C99₁₅₋₅₅ monomer in POPC (blue) and DPC (red). Shaded regions indicate ± 1 standard deviation in uncertainty.

bilayer. This break has previously been identified as a structural GG kink that might be critical in the processing of C99 by γ -secretase.¹⁵ K28 in POPC bilayer and DPC micelle serves as an anchor residue interacting with the lipid headgroups and superficial waters. Simulations using implicit solvent models have suggested that K28 can be involved in critical salt bridges with E22 and D23¹⁴ whose stability might be dependent on the headgroup composition.^{27,28}

Our results (see Figure 4) establish that a structural kink is prominent in the peptide in a micelle environment but less pronounced in the bilayer. Differences in the packing of lipid tail groups in the bilayer and micelle environments, along with substantial surface curvature of the surfactant/solvent interface of the micelle, introduce strain leading to a structural GG kink in the TM helix. In the bilayer there is greater integrity of the JM helix, less interhelical interaction, and a more extended TM helix. In contrast, in the micelle environment there are more substantial fluctuations in the V²³GSN²⁷ region of C99₁₅₋₅₅ (see Figure 4).

An experimental assessment of the distance between the end residues of the TM helix was performed using spin labels at G29 (G700) and L52 (L723) and a pulsed EPR double electron-electron resonance measurement.⁶ Average G29-L52 distances derived from simulation are 34.3 Å in the micelle and 34.5 Å in the bilayer (see Figure 5). The experimentally determined average G29-L52 distances of 33.5 ± 1.0 Å for the WT peptide and 35.3 ± 0.5 Å for the G37L/G38L double mutant peptide (in which the structural kink is expected to be diminished) in 1:4 POPG:POPC lipid vesicles compare well with our simulated results for the POPC bilayer. This is particularly true as it is known that addition of POPG (1-palmitoyl-2-oleoyl-*sn*-glycero-

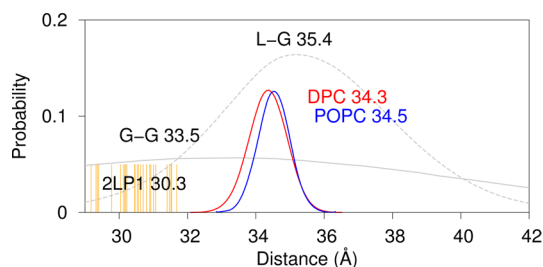


Figure 5. Distribution of distances between the backbone N atoms of residues G29 and L52 derived from all-atom simulations of C99₁₅₋₅₅ in a DPC micelle and POPC bilayer, compared with experimental results derived from EPR studies (dotted line) of spin-labeled C99 in 1:4 POPG:POPC lipid vesicles.⁶ The G29-L52 distance derived from the deposited PDB structures⁶ (orange lines) are found to be significantly shorter than the average distance derived from the EPR data and simulations of C99₁₅₋₅₅ in DPC micelle and POPC bilayer.

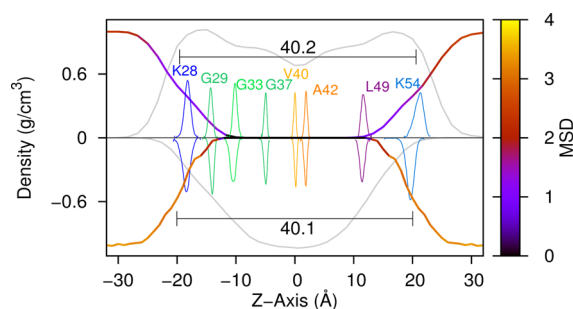


Figure 6. The mass density distribution (gray lines) of the lipid phases for the POPC bilayer (top) and DPC micelle (bottom) derived from all-atom simulations. The water density distribution is colored by the water mean square fluctuation (MSD) as a function of the bilayer normal for POPC and as a function of the distance to the center of the DPC micelle. Superimposed are distributions of C α positions of key residues along the z-axis for C99₁₅₋₅₅ in a POPC bilayer and DPC micelle.

3-phosphoglycerol) to POPC increases the thickness of the lipid vesicle wall.

The degree of GG hinge motion observed in the simulation, while not consistent with the presence of a structural kink in the TM helix, accords well with experimental observations. Based on our simulations, G29-L52 distances in the range of 33–34 Å are inconsistent with the presence of a structural kink in the TM helix near G37/G38. Consistent with this view, the G29-L52 distances derived from the PDB structures (orange lines in Figure 5) lead to a significantly shorter average distance. Interestingly, the distances reported for the WT peptide in 1:4 POPG:POPC lipid vesicles⁶ are consistent with a more modest bend near a hinge located at G37/G38¹⁴ and in agreement with our simulations for the POPC bilayer. Due to the substantial size of the lipid vesicles, the surface curvature is reduced relative to micelles, allowing for a more direct comparison between the vesicle and bilayer results. The uncertainty in the experimental model leads to a broad distribution of distances. However, the center of the distribution is in agreement with simulation results for the POPC bilayer. Results from simulations of C99₁₅₋₅₅ in POPC bilayers and DPC micelles without the CMAP correction (see Figure S1) are consistent with these results.

Profiles of the lipid density in the POPC bilayer and DPC micelle are presented in Figure 6 alongside the related distributions of key residues in the C99₁₅₋₅₅ peptide. In our simulations, the average lipid phase in the POPC bilayer is 40.2

Å, and the widest micelle diameter in the DPC micelle is 40.1 Å (see Methods in SI). While the DPC micelle and POPC bilayer have a small difference in the hydrophobic width, the most significant difference comes from the curvature of the interface shape, which is greater for the micelle. The substantial concavity of the interface facilitates interaction between the JM domain and the TM helix (see Figure S3). Correspondingly, measurable differences are observed in the depths of insertion of particular residues of C99_{15–55} relative to the solvent interface in the bilayer and micelle environments. As shown in Figure 6 (MSD), waters closer to the POPC bilayer interface show smaller MSD values compared to those close to the DPC micelle interface. Given these combined results, it appears that restrained waters at the POPC interface (1) reduce the lipid/solvent interfacial fluctuations and (2) localize and stabilize the C99_{15–55} JM helix relative to the more dynamic surfactant/solvent interface of the DPC micelle.

We have discovered, using simulations of C99_{15–55} monomer in a DPC micelle and POPC bilayer, that the dynamic GG hinge leads to a structural kink in the TM helix. Fluctuations of the TM helix are significantly greater in the spatially constrained DPC micelle than in the POPC bilayer, facilitating enhanced interactions between the JM helical region and the TM helix. This in turn influences helical stability, TM helix extension, exposure to water, and depth of insertion in the lipophilic region. Our results underscore potential differences between the DPC micelle and the POPC bilayer, with the latter more accurately representing a biological membrane. Our simulations suggest that interfacial constraints of the micelle environment place strain on the TM helix and allow for its full extension only with some cost in free energy. The finding that the TM helix under strain forms the structural GG kink at the position of the dynamic hinge near G37/G38 confirms that the extent of fluctuations in the GG kink in the TM helix is controlled by the membrane curvature.^{14,17}

The inherent flexibility in the TM domain may ease its homodimerization and along with the position of a charged residue at K53 may facilitate the positioning of the peptide's *e*-site near the active site of presinillin, the aspartyl protease that forms the active site of γ -secretase, during the initiation of processive cleavage. Flexibility of the TM domain may also facilitate translocation of the peptide during processive cleavage. Moreover, it is likely that termination of cleavage by γ -secretase is determined by the location of charged amino acids flanking the TM-N domain, particularly K28 in WT C99.⁷ Future studies of these questions will impact our fundamental understanding of how C99 processing affects the evolution of AD.

■ ASSOCIATED CONTENT

Supporting Information

This material is available free of charge via the Internet at <http://pubs.acs.org>.

■ AUTHOR INFORMATION

Corresponding Author

straub@bu.edu

Notes

The authors declare no competing financial interest.

■ ACKNOWLEDGMENTS

We acknowledge the support of the National Science Foundation (CHE-1114676 and CHE-0910433) and the

National Institutes of Health (RO1 GM076688). J.E.S. and L.D. thank the Schlumberger Foundation "Faculty for the Future Program" and CONACYT for the generous support of our research. We are also thankful for the resources of the Center for Computational Science at Boston University. This work used the Extreme Science and Engineering Discovery Environment (XSEDE), which is supported by National Science Foundation grant number OCI-1053575.

■ REFERENCES

- (1) Selkoe, D. J. *J. Neuropathol.* **1991**, *53*, 438.
- (2) Hardy, J.; Selkoe, D. J. *Science* **2002**, *297*, 353.
- (3) Kang, J.; Lemaire, H.; Unterbeck, A.; Salbaum, J.; Masters, C.; Grzeschik, K.; Multhaup, G.; Beyreuther, K.; Muller-Hill, B. *Nature* **1987**, *325*, 733.
- (4) Nunan, J.; Small, D. H. *FEBS Lett.* **2000**, *483*, 6.
- (5) Selkoe, D. J. *Physiol. Rev.* **2001**, *81*, 741.
- (6) Barrett, P. J.; Song, Y.; van Horn, W. D.; Hustedt, E. J.; Schafer, J. M.; Hadziselimovic, A.; Beel, A. J.; Sanders, C. R. *Science* **2012**, *336*, 1168.
- (7) Czirr, E.; Cottrell, B. A.; Leuchtenberger, S.; Kukar, T.; TB, T. B. L.; Esselmann, H.; Paul, S.; Schubel, R.; Torpey, J. W.; Pietrzik, C. U.; Golde, T. E.; Wiltfang, J.; Baumann, K.; Koo, E. H.; Weggen, S. *J. Biol. Chem.* **2008**, *283*, 17049.
- (8) Haass, C.; Schlossmacher, M.; Hung, A.; Vigo-Pelfrey, C.; Mellon, A.; Ostaszewski, B.; Lieberburg, I.; Koo, E.; Schenk, D.; Teplow, D. *Nature* **1992**, *359*, 322.
- (9) Seubert, P.; Vigo-Pelfrey, C.; Esch, F.; Lee, M.; Dovey, H.; Davis, D.; Sinha, S.; Schlossmacher, M.; Whaley, J.; Swindlehurst, C. *Nature* **1992**, *359*, 325.
- (10) Masters, C. L.; Simms, G.; Weinman, N. A.; Multhaup, G.; McDonald, B. L.; Beyreuther, K. *Proc. Natl. Acad. Sci. U.S.A.* **1985**, *82*, 4245.
- (11) Iwatsubo, T.; Odaka, A.; Suzuki, N.; Mizusawa, H.; Nukina, N.; Ihara, Y. *Neuron* **1994**, *13*, 45.
- (12) Das, C.; Berezovska, O.; Diehl, T. S.; Genet, C.; Buldyrev, I.; Tsai, J.-Y.; Hyman, B. T.; Wolfe, M. *J. Am. Chem. Soc.* **2003**, *125*, 11794.
- (13) Wolfe, M.; Guénette, S. Y. *J. Cell. Sci.* **2007**, *120*, 3157.
- (14) Miyashita, N.; Straub, J. E.; Thirumalai, D. *J. Am. Chem. Soc.* **2009**, *131*, 17843.
- (15) Beel, A. J.; Mobley, C. K.; Kim, H. J.; Tian, F.; Hadziselimovic, A.; Jap, B.; Prestegard, J. H.; Sanders, C. R. *Biochem.* **2008**, *47*, 9428.
- (16) Miyashita, N.; Straub, J. E.; Thirumalai, D.; Sugita, Y. *J. Am. Chem. Soc.* **2009**, *131*, 3438.
- (17) Pester, O.; Barrett, P. J.; Hornburg, D.; Hornburg, P.; Pröbstle, R.; Widmaier, S.; Kutzner, C.; Dürrbaum, M.; Kapuirniotou, A.; Sanders, C. R.; Scharnagl, C.; Langosch, D. *J. Am. Chem. Soc.* **2013**, *135*, 1317.
- (18) Marrink, S. J.; Risselada, H. J.; Yefimov, S.; Tieleman, D. P.; de Vries, A. H. *J. Phys. Chem. B* **2007**, *111*, 7812.
- (19) Monticelli, L.; Kandasamy, S. K.; Periole, X.; Larson, R. G.; Tieleman, D. P.; Marrink, S.-J. *J. Chem. Theory Comput.* **2008**, *4*, 819.
- (20) Klauda, J. B.; Venable, R. M.; Freites, J. A.; O'Connor, J. W.; Tobias, D. J.; Mondragon-Ramirez, C.; Vorobyov, I.; MacKerell, A. D., Jr.; Pastor, R. W. *J. Phys. Chem. B* **2010**, *114*, 7830.
- (21) Huang, J.; MacKerell, A. D. *J. Comput. Chem.* **2013**, *34*, 2135.
- (22) Ayton, G. S.; Voth, G. A. *Curr. Opin. Struct. Biol.* **2009**, *19*, 138.
- (23) Lyubartsev, A. P.; Rabinovich, A. L. *Soft Matter* **2011**, *7*, 25.
- (24) Marrink, S. J.; de Vries, A. H.; Tieleman, D. P. *Biochim. Biophys. Acta, Biomembr.* **2009**, *1788*, 149.
- (25) Scott, H. L. *Curr. Opin. Struct. Biol.* **2002**, *12*, 495.
- (26) Straub, J. E.; Thirumalai, D. *Annu. Rev. Phys. Chem.* **2011**, *62*, 437.
- (27) Tofoleanu, F.; Buchete, N.-V. *J. Mol. Biol.* **2012**, *421*, 572.
- (28) Poojari, C.; Kukol, A.; Strodel, B. *Biochim. Biophys. Acta, Biomembr.* **2013**, *1828*, 327.
- (29) Licht, S.; Lee, I. *Biochemistry* **2008**, *47*, 3595.